Acta Geochim (2022) 41(6):982–999
https://doi.org/10.1007/s11631-022-00562-x

ORIGINAL ARTICLE

Comparing mineral weathering and elemental transport between earth's critical zone with different parent rocks in Yanshan Mountain, Hebei province, China

Zijian Sun[1,2] · Zhen Liao[3] · Wei Shen[1] · Daqing Fu[4] · Xiaofeng Wei[3] · Huiqiong Zhang[2] · Ziran Chen[2] · Lianghui Xiong[2] · Tianhao An[2] · Hao Wei[5]

Received: 10 May 2022 / Revised: 29 July 2022 / Accepted: 6 August 2022 / Published online: 21 September 2022

Abstract Bedrock weathering performs a significant influence on the evolution of Earth's critical zone. Carbonate rock (dolostone), metamorphic rock (gneiss), and sedimentary rock (sandstone) geological formations in Yanshan Mountain, Hebei Province, are taken as objects to probe the controlling of geological formations on weathering characteristics, migration, and enrichment of elements as well as structure of Earth's critical zone under the identical climate conditions through geological field survey, analysis on minerals component, element distribution in the weathering profile. The dolostone geological formation (DGF) is lithologically dominated by dolostone, characterized by the strongest and predominant chemical weathering. During bedrock weathering and pedogenesis, DGF is marked by significant depletion of CaO, MgO, S, Mn, Mo and enrichment of N, K, Fe_2O_3, and Zn with concentrations of P, Cu, and B keeping stable. Shortage of soil-forming materials and significant loss are driven by soil erosion, which results in thin regolith and soil. The soil thickness is less than 10 cm, and the regolith thickness is less than 30 cm. The vegetation community is predominantly rock arbor or brush, which is calcivorous and tolerant of barrenness. Plagiogneiss is a dominant rock type of gneiss geological formation (GGF), characterized by the weakest weathering and fast chemical and physical weathering rate. GGF is masked by significant depletion of P, K, CaO, MgO, Fe_2O_3, Mn, Cu and enrichment of N, S, Mo, and B, with contents of Zn keeping stable. Both soil and regolith developed in GGF are relatively thick for one of the reasons that biotite expands during weathering. The soil thickness is more than 50 cm, and the regolith thickness ranges from 100 to 200 cm. The vegetation community is predominantly high-quality economic forests and various arbors because of the enrichment of nutrients in GGF. Sandstone is primarily a rock type of sandstone geological formation (SGF), characterized by moderate weathering degree and slow chemical weathering rate. SGF is marked by significant depletion of P, K, CaO, MgO, Fe_2O_3, and enrichment of N, S, Mn, Cu, Zn, and Mo, with fluctuant changes of Zn and B. The thickness of soil developed in SGF varies between that of DGF and GGF. The soil thickness ranges from 30 to 50 cm, and the regolith thickness ranges from 50 to 100 cm. Chinese pines are widely spread on the shady slopes of SGF. Research provides theoretical support for screening dominant ecological resource areas, ecological industry development and ecological protection and restoration for Yanshan Mountain, Hebei Province.

Keywords Yanshan Mountain · Earth's critical zone · Rock weathering · Pedogenesis · Migration and enrichment of element

✉ Zhen Liao
liao_zhen@zijinmining.com

[1] School of Earth Sciences and Resources, China University of Geosciences, Beijing 100083, China

[2] Beijing Institute of Geology for Mineral Resources CO., LTD, Beijing 100012, China

[3] Sino-Zijin Resources CO., LTD, Beijing 100012, China

[4] Hebei Huakan Resource Environmental Survey CO., LTD, Chengde 067060, Hebei, China

[5] Hebei Center for Ecological and Environmental Geology Research, Hebei GEO University, Shijiazhuang 050031, China

1 Introduction

Yanshan Mountain in Hebei province is located in the northern water conservation functional area of Beijing-Tianjin- Hebei region. Nonetheless, there are some prominent eco-environmental issues in which water and soil conservation capacity are weak, and soil erosion is severe (Zhao et al. 2022), which restricts the sustainable development of the social economy to some extent. The Earth's critical zone is defined as the Earth's surface system associated with human economic society, which is the material carrier of the ecological environment. Therefore, it's urgent to improve the understanding of the development and evolution of critical zone, contributing to systematically solving eco-environmental issues and improving eco-environmental quality. Earth's critical zone stemmed from weathering of the parent rock. Under the synthetic action between atmospheric, water, thermal factors and biology, hard parent rocks are broken into loose materials through complex physical and chemical processes, providing the material for the sustainable development of the ecological system, maintenance and evolution of the surface life system (Lü and Li 2006; Yang et al. 2016). Hence, rock weathering performed remarkable influences on the development of Earth's critical zone and the evolution of the ecological system (Brantley et al. 2007; Dixon et al. 2016; Fang et al. 2018; Sun et al. 2020; Xiao et al. 2021).

The geological formation is the paragenetic assemblage of rock characterized by genetic association and similar material composition and structure. Identical geological formations form a similar geological environmental basement (Łukasz et al. 2016; Shi et al. 2019). On the contrary, the characteristics and evolution of the basement, including soil geochemistry, geomorphic landscape, engineering rock group, and hydrogeology, are significantly different between different geological formations. Geological formations take a decisive role in the initial ecological environmental background, including soil and water conditions, topography, geologic hazard and vegetation community (Hahm et al. 2014, 2019). Hence, under identical climate conditions, geological formations remarkably impact the development and evolution of Earth's critical zone and various ecological environments (He et al. 2020; Wang et al. 2020; Wei et al. 2020; Yin et al. 2020; Nie et al. 2021; Zhang et al. 2021). In this paper, dolostone formation(DGF), gneiss formation (GGF) and sandstone formation (SGF) in Xinglong-Kuancheng of Yanshanshan Mountain in Hebei are taken as objects to explore the weathering features, the process of pedogenesis, as well as elements distribution, migration, and enrichment in the critical zone via field survey, sampling of weathering profile, and geochemical analysis. The impacts of geological formation on the development and evolution of Earth's critical zone and vegetation community are researched to provide the geological suggestion for region eco-environmental protection.

2 Study area

2.1 Geographical conditions

The study area is located in the southern Yanshan Mountain, geographically distributed in Kuancheng County and Xinglong County, Hebei Province. Yanshan Mountain is broadly defined to be bounded by North China Plain on the northern, Mongolian Plateau on the southern, Bohai Bay on the western, and Loess Plateau on the eastern, which is hosted in the transition belt of the Inner Mongolia plateau to the North China Plain (Zhao 2007). It is generally characterized by warm temperate semi-humid continental monsoon climate, with a mean annual temperature of ca.10 °C and a monthly mean temperature of −7 °C in December, the coldest month, and monthly mean temperature of 24 °C in July, the warmest month, and with the annual rainfall of ca. 631 mm. The vegetations belong to North China flora, located in the Chinese-Japanese subregion, the Holarctic region. The typical dominant tree species are broadleaf forests consisting of *Quercus Mongolica Fisch and Populus tremula Var, davidiana Schneid*, coniferous *Pinus tabulaefomis Carr*. In addition, Shrubs are widespread, dominated by *Vites incise Bunge, Spiraea trilobata Linn, Zizyphus spinosus Hu* and *Corylus heterophylla Fisch*.

2.2 Geology setting

The study area is tectonically located in the Mesozoic continental volcanic sedimentary basin, Yanshan intraplate orogenic belt, the southern margin of the North China continent (Zhang et al. 2014; Guan et al. 2018). The strata lithologies in the area are dominated by carbonate, clastic rocks, metamorphic rocks and igneous rock: (1) Mesoproterozoic Jixian group Wumishan Formation (J*xw*) and Changcheng Group Gaoyuzhuang Formation (Ch*g*) dolomicrite, sandy dolostone, crystal powder dolostone; (2) Changcheng Group Changzhougou Formation (Ch*c*) and Dahongyu Formation (Ch*d*) quartz sandstone, Chuanlinggou Formation (Ch*ch*) silty shale, fine sandstone, siltite, as well as Qingbaikou System Xiamaling Formation (Qn*x*) mudrock, shale, siltite; (3) Neoarchean Xiaoguanzhuang Formation (Ar_3gn) and Zunhua Group-complex (Ar_3z) plagioamphibolite, amphibole plagio-gneiss, mixed up with amphibole plagio- granulite; (4) Jurassic Baihuashan (J_3B)

slablike quartz monzonite, Huangliang (J_3HL) slablike quartz monzonite and Lishuyu (J_1L) medium-fine grained quartz monzonite (Fig. 1a). According to lithology and mineral components, dolostone geological formation (DGF), gneiss geological formation (GGF), and sandstone geological formation (SGF) are predominant geological formations, which cover an area about 1645 km^2, 907 km^2, and 1577 km^2 respectively (Fig. 1b).

3 Material and methodology

3.1 Sampling and chemical analysis

A reconnaissance survey along all available access roads allows for selecting representative exposures for detailed observation and sampling. A total of 45 critical zones are selected from three kinds of geological formations in the region, comprising 20 critical zones in DGF, 16 critical zones in GGF, and 9 critical zones in SGF. Multiple samples are systematically collected along a profile going from bedrock (firm, unaltered or slightly altered protolith) to regolith (weak, brittle, altered rock material with the texture and structure of the bedrock) and eventually soil material for petrographic, geochemical and mineralogical analyses, including a total of 92 samples in DGF, 85 samples in GGF, and 38 samples in SGF (Fig. 1b).

Each soil sample is a mixture of 3–5 plots collected in the manner of "S" or "X" and crushed into ten mesh for major and trace element geochemical analysis and X-ray diffraction analyses. Multiple soil samples are taken at intervals of 20 cm in thick soil. The regolith sample is also a mixture of 3–5 plots within the scope of 5–10 m in the same regolith layer. Bedrock sample is the mixture of 3–5

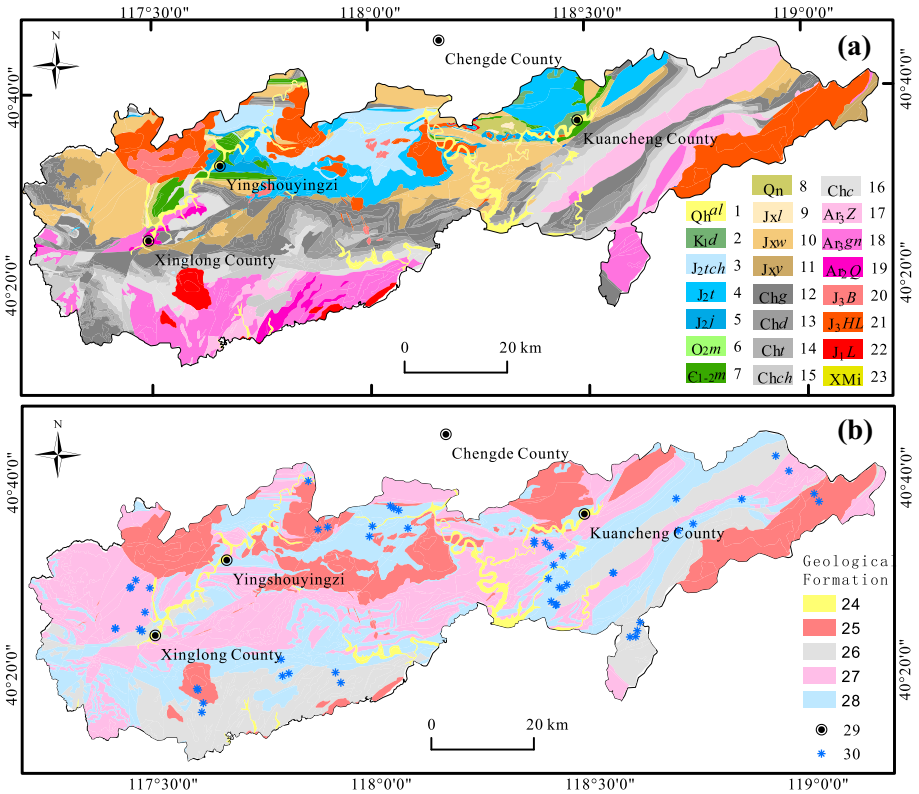

Fig. 1 Regional geological map **a** and Regional geological formation map **b** (modified from 1:250,000 regional geological map) 1. Holocene epoch; 2. Cretaceous Dabeigou Formation; 3. Jurassic Houcheng Formation; 4. Jurassic Tijishan Formation; 5. Jurassic Jiulongshan Formation; 6. Ordovician Majiagou Formation; 7. Cambrian Mantou Formation; 8. Neoproterozoic Qingbaikou Group; 9. Mesoproterozoic Jixian Group Tigerding Formation; 10. Mesoproterozoic Jixian Group wumishan Formation; 11. Mesoproterozoic Jixian Group Yangzhuang Formation; 12. Mesoproterozoic Great Wall Group Gaoyuzhuang Formation; 13. Mesoproterozoic Great Wall Group Dahongyu Formation; 14. Mesoproterozoic Great Wall Group Tuanshanzi Formation; 15. Mesoproterozoic Great Wall Group Chuanlinggou Formation; 16. Mesoproterozoic Great Wall Group Changzhougou Formation; 17. Neo-archean Zunhua Group; 18. Neo-archean Zunhua Group Xiaoguanzhuang Gneiss; 19. Mesoarchean Qianan Group; 20. Jurassic Baihuashan quartz monzonite; 21. Jurassic huangliang porphyritic quartz syenite; 22. Jurassic Lishuyu Medium and fine-grained monzonitic granite; 23. Xinglong Migmatite; 24. Quaternary; 25. Igneous rock geological formation; 26. Dolostone geological formation; 27. Gneiss geological formation; 28. Sandstone geological formation; 29. Geographical location; 30. Sampling location

plots within the scope of 5–10 m in the identical lithologic unit, partly crushed into 200 mesh for geochemical analyses of major and trace elements and partly made into 30 μm-thick standard thin sections for petrographic analyses. SiO_2, Al_2O_3, TFe_2O_3, MgO, CaO, Na_2O, K_2O, Mn, Ti, P and S are analyzed by Wavelength dispersive X fluorescence spectrometer (WDX) and other trace elements by ICP-OES (PE, USA) in Test Center of 514 brigade of north China geological exploration bureau Co., Ltd. The analytical quality is controlled by several control samples in each analytical batch of samples, including reference material (GBW) for checking the accuracy and reproducibility of the method and 10% duplicated samples for checking precision. Both accuracy and precision for all the elements studied are accepted.

3.2 Statistical analysis and weathering index

(1) The data are statistically analyzed by SPSS 26.0 to explore the element distribution features in the bedrock-regolith-soil continuum of Earth's critical zone in three kinds of geological formations. R-mode factor analysis is used to interpret a large number of measured variables by reducing them to a smaller number of independent, theoretical variables (factors), therefore R-mode factor analysis is performed for geochemical associations R-mode factor analysis.

(2) Composite weathering index (CWI), multi-index and recapitulative, is applied to measure the weathering degree based on that weathering process is essentially the migration and enrichment of elements. CWI reflected the variances of weathering degree compared with parent rock so that it can be applied to probe the evolution of weathering degree from bedrock to soil. The Eq. (1) is as follows:

$$\mathrm{W} = \left[1 - \frac{E' * \bar{t} + E}{2}\right] \times 100\% \quad (1)$$

In Eq. (1), E' is the equilibrium degree of three kinds of weathering rate indexes, including SiO_2/Al_2O_3, Al_2O_3/Fe_2O_3 and $(Al_2O_3 + Fe_2O_3)/SiO_2$. t is the mean value of the leaching coefficient of five types of oxide, including SiO_2, CaO, MgO, K_2O, Na_2O. E is the equilibrium degree of seven kinds of oxide's variable coefficient, including SiO_2, Al_2O_3, F_2O_3, CaO, MgO, K_2O, Na_2O. The calculation method is detailed and described by Huang (1996).

(3) Mass transfer coefficient, τ, as a tool in quantificationally measuring the quantity of element migration and enrichment, is well defined and widely accepted (Chadwick et al. 1990; Anderson et al. 2002). Ti is selected as an immobile reference element to calculate τ of other elements (Zhou et al. 2005). $\tau > 0$ infers that the element enriched in the weathering and pedogenesis, whereas the element migrated and depleted. The Eq. (2) is as follows:

$$\tau = [(C_{j,w}/C_{j,p}) \times (C_{i,p}/C_{i,w}) - 1] \times 100\% \quad (2)$$

where C_j and C_i are the concentration in weight percent of element j and immobile element i, and the subscripts w and p refer to weathered material and parent rock, respectively.

4 Results and discussion

4.1 Rock weathering and pedogenesis

4.1.1 Mineralogy

As the study area has long been situated in a relatively stable tectonic setting, bedrock geology played a decisive role in the pedogenesis and evolution of Earth's critical zone under identical climate conditions. Mineralogical composition, structure and cement type exerted significant impacts on soil-forming material, physical and chemical weathering features, e.g., weathering type, weathering strength, weathering rate, as well as soil erosion rate (Zhang and Li 1990; Yuan et al. 2010; Fu et al. 2021).

As the parent materials of DGF, fresh dolostone samples principally consist of powdery dolomite, micritic dolomite and a low quantity of terrigenous sandy clastic materials (Fig. 2a). Dolostone is slightly fragmental, with fractures being filled with dolomite and opaque mineral (Fig. 2d). Plagiogneiss is the dominant parent rock type of GGF, whose mineral compositions are plagioclase, quartz, amphibole, biotite, and garnet (Fig. 2b). Plagioclase is moderately altered to sericite or opaque minerals. Biotite and amphibole are oriented distributed, and slightly altered to chlorite or opaque minerals along mineral fissures or margins (Fig. 2e). Sandstone is the primary parent rock type of SGF, composed of sandy fragments and interstitial material. The former is mainly subangular rock debris, quartz and feldspar, slightly oriented distributed, with a size of 0.05–0.1 mm. Feldspar is primarily plagioclase, somewhat altered to sericite or opaque minerals. Rock debris comprised sericitization alteration rock, siliceous rock, and less quantity of mica. The latter is dominated by sericitization clay mixed base and siliceous rock (Fig. 2f).

The mineralogical compositions of soil samples are significantly different between three kinds of geological formations (Table 1). The most abundant minerals are feldspars in all soil samples, maybe as a result of relatively weak weathering in the region. Another main component is quartz, which is weather-resistant and reserved in the soil after weathering. Some dolomite and calcite are detected in DGF but absent in the soil samples of GGF and SGF. Silicates are occasionally detected and composed of mica,

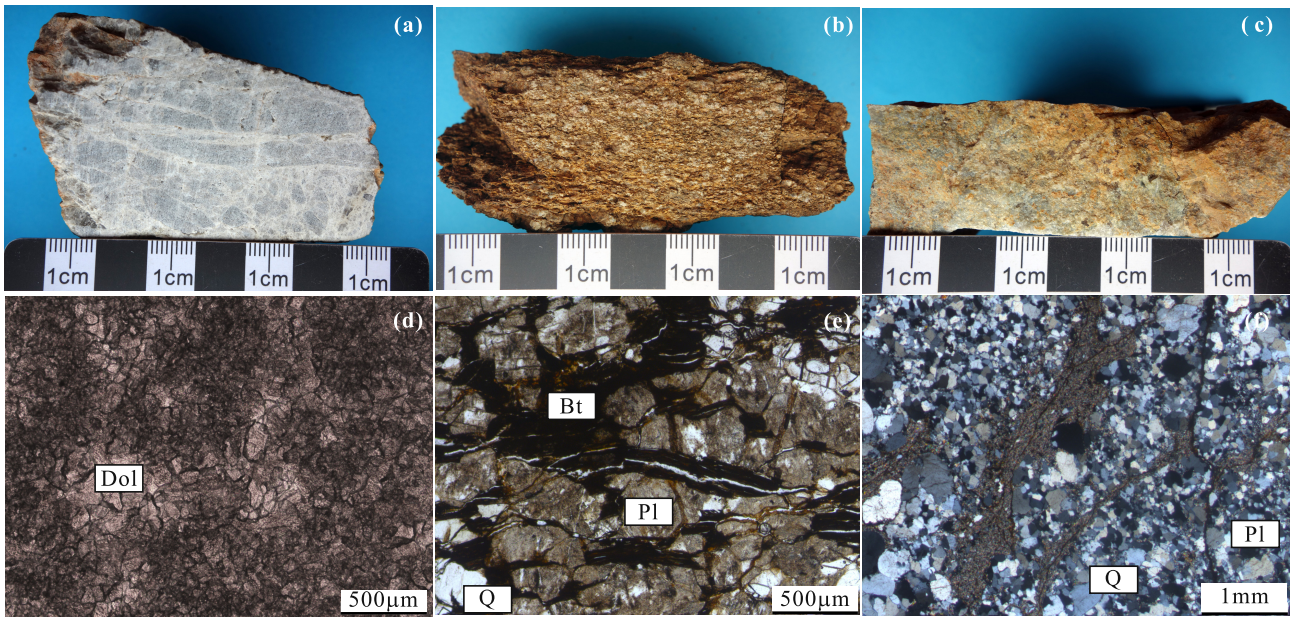

Fig. 2 Bedrock sample photos and electron photomicrograph of Yanshan Mountain **a**. Dolostone sample photo; **b**. Gneiss sample photo; **c**. Sandstone sample photo; **d**.Dolostone electron photomicrograph; **e**. Gneiss electron photomicrograph; **f**. Sandstone electron photomicrograph; Dol. Dolomite; Pl. Plagioclase; Q. Quartz; Hb. Hornblende; Bt. Biotite

Table 1 Major mineral composition of soils in Yanshan Mountain

Geological Formation	DGF						GGF			SGF		
Quartz	21.8	28.9	14.0	21.8	18.32	22.9	9.83	10.8	11.6	19.9	27.8	18.6
Feldspar	49.6	29.2	22.4	47.2	29.2	45.6	49.1	54.5	38.9	54.7	45.4	49.2
Dolomite	6.91	19.1	37.2	12.9	20.1	3.51	–	–	–	–	–	–
Calcite	–	6.88	–	–	11.7	2.81	–	–	–	–	–	–
Mica	2.63	2.89	2.63	2.68	3.26	2.45	1.86	2.48	2.18	4.02	3.02	4.98
Chlorite	2.05	–	1.98	3.05	4.01	2.04	–	2.16	–	2.86	2.94	2.77
Pyroxene	3.26	–	–	3.93	–	–	4.46	3.95	4.18	5.11	3.61	3.15
Amphibole	1.22	0.820	0.320	1.61	0.690	–	9.66	10.5	2.65	2.09	1.12	2.69
Hematite	1.89	–	–	4.12	3.85	4.86	–	–	4.12	3.02	3.91	5.74
Smectite	10.6	9.41	18.2	2.69	8.92	15.8	21.5	15.7	27.4	8.29	12.1	13.1
Kaolinite	–	2.85	3.34	–	–	–	3.57	–	3.92	–	–	–
Unknown	–	–	–	–	–	–	–	–	5.00	–	–	–

chlorite, pyroxene and amphibole, in which amphibole is richer in GGF than SGF and DGF. Hematite is the dominant iron oxide in the region as it is preferentially formed in drier and warmer conditions (Clift et al. 2014). Smectite is the predominant clay mineral in all soil samples, consistent with arid regions being less leaching and dominantly developing smectite-rich soil (Clift et al. 2014). There are still low quantities of Kaolinite in soil samples of DGF and GGF, but it is absent in soil samples of SGF.

4.1.2 Weathering characteristics

Composite weathering index(CWI) gradually declined with weathering depth increasing from soil to regolith in both weathering profiles of DGF and SGF. Nevertheless, CWI of soil is generally more significant than that of regolith, while CWI is characterized by a slight fluctuation in the profile of GGF. In general, CWI is demonstrated as an effective proxy for rock weathering strength. Regarding weathering strength of three kinds of geological formations, the CWI of DGF is more significant than that of SGF and much larger than that of GGF (Table 2). It is proven that in acid soil, the mineral sequence resistant to weather

Table 2 Summary of CWI of Earth's critical zone in Yanshan Mountain

Profile	DGF			GGF			SGF		
	Median	Ave	*P* value	Median	Ave	*P* value	Median	Ave	*P* value
Weak weathering regolith	42.6 (8.30–52.7)	35.2	0.093	38.4 (3.70–48.0)	26.8	0.004	8.9 (2.10–31.1)	14.0	0.239
Strong weathering regolith	42.5 (16.8–51.4)	35.9	0.011	38.3 (6.30–47.0)	27.4	0.001	37.7 (11.9–43.2)	30.4	0.338
Deep soil	39.8 (30.4–53.5)	40.9	0.141	38.6 (27.3–42.6)	33.8	0.000	42.7 (37.5–45.2)	38.7	0.000
Topsoil	43.2 (33.3–53.5)	43.2	0.614	38.4 (37.4–42.5)	34.0	0.000	42.1 (37.0–51.3)	40.7	0.043

is respectively in the following order: carbonate minerals < chlorite < biotite < amphibole < pyroxene < plagioclase < potash < Muscovite < vermiculite < quartz (Hodson et al. 1996; Xu and Ma 2002; Lo et al. 2017) so that the weathering rate of rocks, widespread in nature, declined according to the order of carbonate rock, basalt, granite, and sandstone respectively (Meybeck 1987; Sun 2018). In general, a faster weathering rate contributes to more substantial weathering. Nonetheless, weathering strength of GGF is also controlled by the rapid soil erosion rate, resulting in weaker weathering of profiles, which is proposed as the 'weathering limit'. According to the summary of soil erosion characteristics in Haihe river basin, Shanxi province, adjacent to Hebei province, the soil developed in gneiss is characterized by thick regolith and soil, low content of clay and looseness of structure, resulting in its being prone to erosion (Zhang et al. 1991). In terms of specific data, ^{137}Cs tracer and soil erosion model are applied to measure the soil erosion rate of gneiss in Yimeng Mountain, Shandong province, indicating the moderate-strong soil erosion of gneiss (Zhang et al. 2011). Furthermore, in the study area, the organic matter in gneiss varies between 0.20 and 4.69, with an average of 1.85. In conclusion, rapid erosion rates of GGF dominantly result from loose texture and low content of clay and organic matters.

$A1_2O_3$-CaO* + Na_2O-K_2O (A-CN-K) diagram has empirically and kinetically predictable weathering vectors for various minerals and rock types (Nesbitt and Young 1984). According to the mobility of elements, the chemical weathering process is sorted into three stages: migration of Na and Ca, migration of K, eventually migration of Si and enrichment of Al (Nesbitt and Young 1984; Li et al. 2007; Gu et al. 2021). As predicted for three kinds of geological formations, the majority of the samples in the profile of GGF followed a weathering trend that is adjacent to the A–CN join (Fig. 3b), while that of DGF reached more closed to the A apx (Fig. 3a), and that of SGF showed more dissolution of K-feldspar (Fig. 3c). We conclude that the chemical weathering of GGF is dominantly at the stage of migration of Na and Ca, that of SGF is preliminary at the stage of migration of K, and that of DGF had a faster rate of aluminous weathering products conservation. However, CIA is applied to represent feldspar's chemical alteration degree to clay minerals (Nesbitt and Young 1984). In general, decomposition of feldspar results in the loss of alkali and alkali earth metals, such as Na, K, and Ca, accompanied by the formation of clay minerals and enrichment of Al. However, in the DSF, the enrichments of alkali metal and alkali earth metal in soil result in decreased CIA. K may participate in forming clay minerals, such as illite at the early stage of weathering, and be retained in the soil as a composition of mica. In addition, K and Na have been retained in weathering profile probably by being absorbed by clay minerals or under the influence of biological behaviors (Jin et al. 2010). Thus, CIA is probably not appropriate to represent the weathering degree of DGF; hence, CIW was applied to measure the weathering degree of three geological formations.

4.1.3 The weathering and pedogenesis process

Under the semi-arid and semi-humid monsoon climatic conditions, with an annual rainfall of ca. 631 mm and large interannual variability, evaporation is far greater than precipitation. Atmospheric precipitation ran off mainly as the surface flow and the absence of water infiltrating into soil resulted in weak eluviation of soil in the region. Hence, the impacts of climate on parent rock weathering are unremarkable (Zhang and Li 1990). The impacts of climate on soil are the hydrothermal conditions and the organic matter accumulation in the soil through their control of vegetation growth. As the dominant clay mineral, smectite is generally formed under warm and seasonally arid conditions, which is the dominant clay mineral in all soils of three kinds of geological formations (Hong et al. 2012). Rock weathering is dominated by physical weathering in the region (Ma et al. 2003), accompanied by relatively weak chemical and biological weathering. Chemical weathering is at the early kaolinization stage in the lateralization process, with the formation of abundant smectite but a minority of kaolinite in soil. From the perspective of

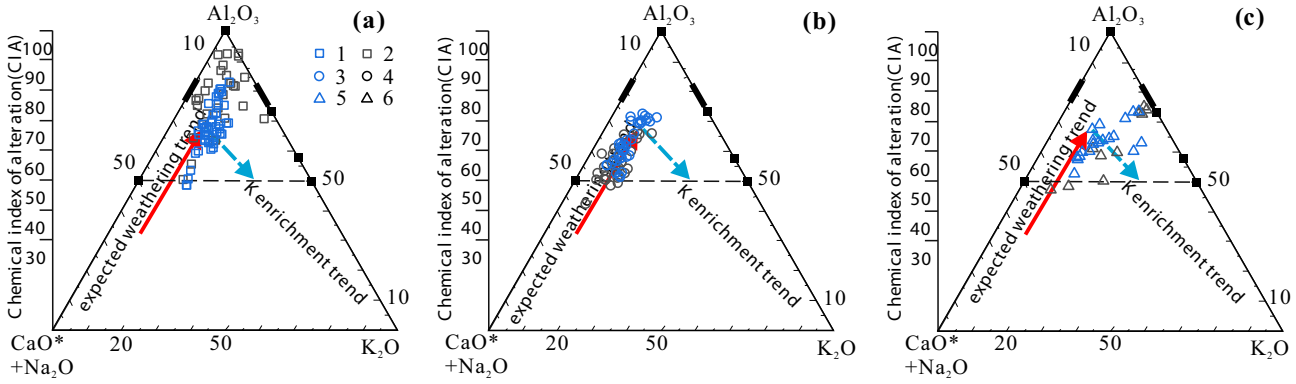

Fig. 3 Diagram of $A1_2O_3$-CaO* + Na_2O-K_2O (A-CN-K) 1. Soil samples of DGF; 2. Regolith samples of DGF; 3. Soil samples of GGF; 4. Regolith samples of GGF; 5. Soil samples of SGF; 6. Regolith samples of SGF

three kinds of geological formations' weathering features, chemical weathering played a dominant role during weathering and pedogenesis of DGF because dolomite is the single mineral component. Although dolostone is stronger weathering than gneiss and sandstone, lack of soil-forming materials and high soil erosion relative to weathering products lead to thin regolith and soil in DGF. Gneiss had complicated and diverse minerals, such as plagioclase, biotite and hornblende, so that gneiss is amenable to physical weathering and a fast chemical weathering rate. Thus, thick regolith and soil are dominantly developed in GGF. Nonetheless, the soil structure is loose, and for finer-grained, lower density minerals such as clays, the lag between erosion and deposition on the slope may be much less as they are carried rapidly by soil erosion. In addition, the water–rock reaction is insufficient and unaltered feldspar is rich in soil, resulting in weaker weathering of sustainably young soil (Chen 2019). Quartz is abundant in SGF, which is more resistant to weathering and keeps stable according to the Goldich dissolve sequence (Goldich 1938). Cement dissolving and feldspar alteration are implicated during weathering of SGF, with quartz keeping the same size and shape (Liao 1997), and eventually, the weathering rate of sandstone is slow (Spatti júnior et al. 2019). The slow weathering rate and moderate weathering strength result in the heterogeneity of regolith and soil thickness of SGF, which are between that of DGF and GGF in general.

4.2 Weathering influences migration and enrichment of elements in earth's critical zone

4.2.1 Distribution of elements characteristics

In general, the soil is characterized by illuviation of parent materials, as the soil is developed by in situ weathering of parent rock in the mountainous area. Minerals composition, element association, and weathering degree of parent rock determined the geochemical features of soil to some extent. Contents of nutrient elements in soil covary strongly with that in parent rock for the strong affinity of geochemical elements (Brantley et al. 2007; Hewaisam et al. 2013; Cheng et al. 2019; Sun et al. 2020).

Macronutrients, including total nitrogen (TN), total potassium (TK) and sulfur (S), together with micronutrients comprising boron (B) and molybdenum (Mo), are richer in the soil of SGF than that of DGF and GGF. Potassium feldspar and mica are dominant K-rich minerals (Li et al. 2013), allowing the enrichment of K in the soil of SGF. Macronutrients CaO is most abundant in the soil of DGF, in accord with the dolomite and calcite being reserved in the soil. Nevertheless, Macronutrients MgO is slightly more affluent in the soil of GGF than that of DGF and SGF, as a consequence of MgO occurring as isomorphism in clay minerals and being retained in the soil of GGF. Macronutrients, including total phosphorus (TP), together with micronutrients, including iron (Fe_2O_3), manganese (Mn), Copper (Cu) and Zinc (Zn), are richer in the soil of GGF than that of SGF and DGF. Fe_2O_3 and Mn are mainly derived from biotite, hornblende and Hematite, which are enriched in the soil of GGF. In addition, a minority of Fe^{2+} may occur as isomorphism in clay minerals together with Mg^{2+}. It is worth noting that size rules of multiple nutrient contents in soil, such as TN, TP, CaO, Fe_2O_3, Mn, Cu and Zn, bear notable similarity and uniformity with regolith and bedrock compared within the corresponding layer of three kinds of geological formations. For example, TP is more abundant in bedrock, regolith and soil of GGF than in the corresponding layer of DGF and SGF. The strong covariation between nutrient content in soil and parent rock argues for the inherent origin of soil nutrients from parent rock (Table 3 and Fig. 4). On the contrary, the differences between nutrient

Table 3 Summary of nutrients content of Earth's critical zone in Yanshan Mountain

Profile	Elements	DGF	GGF	SGF	Elements	DGF	GGF	SGF
Soil	TN[a]	1980 (950–3009)	929 (446–1245)	2828 (1087–3353)	Mn[a]	599 (390–682)	652 (548–919)	599 (385–815)
Regolith		312 (185–473)	137 (103–214)	337 (148–406)		185 (86.4–550)	621 (414–766)	230 (51–447)
Bedrock		122 (96–145)	93.5 (87.3–117)	140 (90–175)		78 (44.3–122)	646 (516–822)	297 (41.5–633)
Soil	TP[a]	460 (269–700)	656 (443–1024)	624 (426–969)	Cu[a]	22.6 (18.4–32.3)	60.2 (41.5–67.3)	24.8 (15.7–28.3)
Regolith		188 (96.7–282)	875 (605–1335)	530 (240–654)		10.8 (3.92–20.9)	37.6 (25.8–53.7)	9.62 (2.68–28.8)
Bedrock		53.8 (39.9–114)	964 (502–1406)	489 (93–1062)		2.98 (2.16–6.57)	49 (25.91–63)	13.5 (2.35–20.7)
Soil	TK[a]	16,188 (12,390–22,277)	15,727 (13,600–17,848)	22,746 (20,156–30,582)	Zn[a]	62.3 (54.2–71)	91.9 (73.6–101)	73.9 (54.9–86.7)
Regolith		4862 (1973–11,549)	17,607 (13,697–20,322)	25,303 (16,308–30,333)		13.6 (11.9–45)	75.9 (57.4–92.3)	37.8 (7.06–71.8)
Bedrock		608 (418–3642)	18,500 (14,218–21,716)	11,896 (9601–28,652)		9.03 (2.54–12.4)	70.2 (52.5–86.1)	46.3 (5.67–68.3)
Soil	CaO[b]	3.71 (1.78–7.59)	1.88 (1.05–2.85)	1.13 (0.591–1.81)	Mo[a]	0.731 (0.638–0.871)	0.425 (0.318–0.527)	0.774 (0.549–0.907)
Regolith		18.8 (16.4–24.8)	3.1 (1.32–4)	0.551 (0.167–1.37)		0.321 (0.192–0.692)	0.2 (0.151–0.283)	0.24 (0.183–0.76)
Bedrock		26.39 (21.2–31)	2.87 (1.34–4.42)	0.364 (0.114–3.06)		0.185 (0.107–0.279)	0.166 (0.145–0.198)	0.35 (0.106–0.551)
Soil	MgO[b]	3.24 (2.1–6.13)	3.46 (2.87–4.41)	1.6 (1.09–2)	B[a]	39.9 (32.8–45)	16.1 (5.8–24.6)	39.9 (29–70.9)
Regolith		13.9 (3.84–19.6)	3.95 (2.61–5.39)	1.29 (0.832–2.04)		18.3 (9.25–37.4)	4.96 (3.2–16)	59.7 (33.2–87.6)
Bedrock		18.4 (13.91–21.7)	3.31 (2.55–4.91)	1.42 (0.318–2.6)		5.51 (2.28–12.5)	6.51 (4.81–10.9)	27 (11.6–56.4)
Soil	Fe_2O_3[b]	4.68 (3.97–5.04)	8.14 (6.82–9.19)	5.37 (4.47–5.63)	S[a]	241 (163–388)	151 (128–180)	314 (145–483)
Regolith		1.33 (0.889–3.35)	7.81 (6.25–8.88)	2.96 (1.12–6.99)		106 (75.2–119)	83.7 (63.5–120)	65.3 (44.8–161)
Bedrock		0.527 (0.196–1.17)	7.17 (6.25–8.21)	4.2 (0.846–6.39)		86 (65.9–112)	78.6 (59.4–100)	70.1 (46.4–81.5)

a. $\times 10^{-6}$; b. %

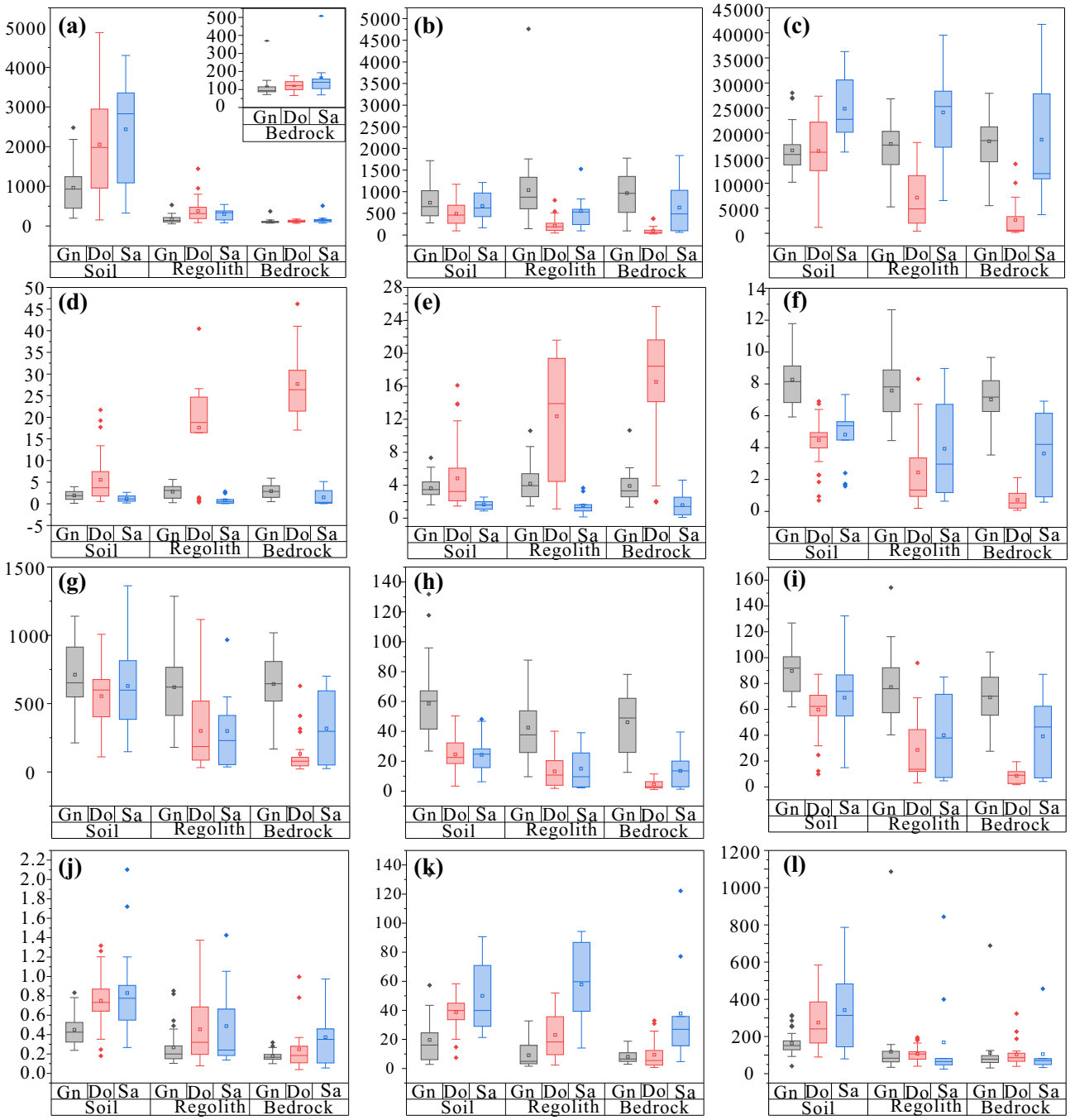

Fig. 4 Box plot of soil nutrients content of Earth's critical zone in Yanshan Mountain **a**. TN ($\times 10^{-6}$); **b**.TP ($\times$ 10–6^{-6}); **c** TK ($\times 10^{-6}$); **d**. CaO (%); **d**. MgO (%); **f**. Fe_2O_3 (%); **g**. Mn ($\times 10^{-6}$); **h**. Cu ($\times 10^{-6}$); **i**. Zn ($\times 10^{-6}$); **j**. Mo ($\times 10^{-6}$); **k**. B ($\times 10^{-6}$); **l**. S ($\times 10^{-6}$). Gn. gneiss; Do. dolostone; Sa. sandstone

content in three kinds of soil are decreased, driven by homogenization and redistribution of elements during weathering and the supergene geochemical process. Homogenization is defined as the result of the lateral migration of elements during weathering and pedogenesis, which is the primary geochemical behavior in the supergene system. From the perspective of element content, if the standard deviation of element content in soil is lower than that in bedrock, it shows that the homogenization of the element occurred. Moreover, the degree of homogenization can be measured by the ratio of the standard deviation of element content in soil to that in bedrock (Hao et al. 2004, 2005). In DGF, only Mg and Ca are homogenized, with the degree of 0.538 and 0.676, respectively. In

GGF, homogenization occurred to Zn, K, P, Mg, Ca and S according to the decreasing order of homogenization degree. In SGF, homogenization occurred to Cu, Zn, Fe, B, P, K, Ca and Mg according to the decreasing order of homogenization degree.

4.2.2 Migration and enrichment characteristics of elements

Bedrock weathering performed remarkable impacts on the vertical variation trends of elements contents in the critical zone as the geochemical process of weathering is essentially the migration and enrichment of elements. according to weathering strength and depth, weathering profile is classified into top-soil, deep soil, strong weathering regolith, weak weathering regolith and bedrock. Bedrock is taken as the unweathered samples to calculate the mass transfer coefficient (Table 4 and Fig. 5). Elements presented different vertical variation rules.

In all three kinds of geological formations, TN content gradually increases from regolith to soil because nitrogen derived from the atmosphere and enriched in soil by biological nitrogen fixation. In both profiles of GGF and SGF, TP content gradually decreases from regolith to soil. Nonetheless, it keeps stable in the profile of DGF. In both profiles of GGF and SGF, TK content shows a gradual decrease from regolith to soil. Nonetheless, it gradually increases in the profiles of DGF. CaO presented significant depletion in all three kinds of geological formations, with the greatest depletion in the profiles of DGF. MgO showed remarkable depletion in the profiles of DGF, but enrichment in regolith and depletion in the soil both of GGF and SGF. S revealed remarkable depletion in the profile of DGF but gradual enrichment from regolith to soil in the profiles of GGF and depletion in regolith and enrichment in the soil of SGF, respectively. Fe_2O_3 gradually enriched during the dolostone weathering process but migrated and lost in both GGF and SGF. Mn generally showed slight depletion in both DGF and GGF but significant enrichment in the profile of SGF. Micronutrients shows different degree of enrichment in soil or keep stable in the profile except for Mo in DGF, whose concentrations are influenced by contents of clay minerals or Fe hydroxide, as well as pH value since they are always absorbed by clay minerals or Fe hydroxide.

In sum, three kinds of geological formations present remarkable vertical variation trends. DGF is characterized by significant depletion of CaO, MgO, S, Mn, Mo and enrichment of N, K, Fe_2O_3, Zn with contents of P, Cu and B keeping stable. GGF is characterized by significant depletion of P, K, CaO, MgO, Fe_2O_3, Mn, Cu and enrichment of N, S, Mo and B, with contents of Zn keeping stable. SGF is characterized by significant depletion of P, K, CaO, MgO, Fe_2O_3, and enrichment of N, S, Mn, Cu, Zn, Mo, with fluctuant changes of Zn and B.

4.2.3 Migration and enrichment processes of elements

The KMO test coefficient of elements in weathering profile of DGF and SGF are 0.831 and 0.665, respectively, and both significance test P values of Bartlett's test of Sphericity are less than 0.01, suggesting that R-mode factor analysis is available for both DGF and SGF. Nonetheless, the KMO test coefficient of elements in weathering profile of GGF is less than 0.6, while the KMO test coefficient of mass transfer coefficient of elements is 0.819, and the significance test P value of Bartlett's test of Sphericity is less than 0.01. Thus, contents or mass transfer coefficients of SiO_2, TiO_2, Al_2O_3, Fe_2O_3, MgO, MnO, CaO, Na_2O, K_2O and P_2O_5 are selected to perform R-mode factor analyses for geochemical associations in DGF, SGF and GGF respectively. Principal component analysis and varimax are adopted to obtain varimax factors. Each varimax factor reflected geochemical associations of closely correlated elements and eventually manifested the geochemical evolution feature, e.g., migration, enrichment and fractionation of elements and geochemical process during weathering and pedogenesis.

Three varimax factors of DGF accounted for 91.8% of the total variance of 10 variables studies (Table 5). Varimax factor 1 (F1), dominantly composed of SiO_2, Ti_2O, Al_2O_3, Fe_2O_3, K_2O, CaO, and MgO, described most of the variations, which clearly indicated the overwhelming effects of parent materials on the concentrations of these elements. SiO_2, Ti_2O, Al_2O_3, $Fe_2O_3$and K_2O are positively associated with factor 1, except CaO and MgO, which are negatively associated with factor 1. It revealed the main weathering and pedogenesis in dolostone characterized by remarkable depletion of CaO, MgO and enrichment of SiO_2, Al_2O_3, Fe_2O_3 and K_2O. SiO_2 and Al_2O_3 comprised phyllosilicate minerals. Enrichment of K_2O is associated with SiO_2, driven by the development and evolution of clay minerals. Factor 2 (F2) and factor 3 (F3) mainly comprised Na_2O, P_2O_5, K_2O, and MnO, P_2O_5, respectively, suggest other effects on the status of these elements, such as the supergene biogeochemical process.

It is proposed that weathering and pedogenesis of carbonate are divided into two stages. In the first stage, the foreign and insoluble substances of bedrock gradually accumulated to form saprolite that continued to weather and pedogenesis similar to other rocks in the second stage (Wang et al. 1999, 2015). The geochemical process of carbonate weathering and pedogenesis is also divided into three stages, e.g., stage of Si-Al- enrichment and Ca-Mg-depletion, stage of Fe- Mn- enrichment, stage of Al-enrichment and Si-depletion. (Zhu and Li 2006; Qiu et al.

Table 4 Nutrient element-mass-transfer coefficient of Earth's critical zone in Yanshan Mountain

Profile	Elements	Mass transfer coefficient (τ)			Elements	Mass transfer coefficient (τ)		
		DGF	GGF	SGF		DGF	GGF	SGF
4	TN	1.82 (0.058–5.18)	7.63 (3.98–11.9)	6.92 (2.73–17.4)	Fe_2O_3	0.054 (−0.278–0.461)	−0.169 (−0.256–0.034)	−0.156 (−0.578–−0.055)
3		0.466 (−0.013–2.71)	3.77 (1.33–5.72)	3.64 (1.87–11.8)		0.125 (−0.155–0.412)	−0.125 (−0.224–−0.034)	−0.108 (−0.548–−0.033)
2		−0.007 (−0.764–0.698)	0.459 (−0.067–1.34)	0.183 (−0.412–0.461)		−0.043 (−0.25–0.189)	−0.01 (−0.074–0.119)	−0.057 (−0.342–0.073)
1		−0.329 (−0.781–0.032)	0.243 (−0.238–0.411)	0.21 (0.049–3.82)		−0.013 (−0.393–−0.002)	0.032 (−0.104–0.145)	−0.007 (−0.216–0.383)
4	TP	0.036 (−0.533–0.361)	−0.495 (−0.628–−0.102)	−0.174 (−0.601–0.413)	Mn	−0.057 (−0.682–0.304)	−0.178 (−0.382–0.113)	0.154 (−0.118–1.58)
3		−0.117 (−0.674–0.228)	−0.377 (−0.693–−0.141)	−0.19 (−0.622–0.219)		−0.2 (−0.672–0.181)	−0.172 (−0.381–−0.074)	−0.017 (−0.186–0.82)
2		0.133 (−0.637–0.672)	−0.171 (−0.348–0.039)	0.031 (−0.468–0.635)		−0.182 (−0.657–0.288)	−0.148 (−0.481–0.199)	−0.163 (−0.334–0.043)
1		−0.114 (−0.809–0.212)	0.078 (−0.074–0.537)	0.276 (−0.011–5.075)		−0.515 (−0.754–−0.199)	−0.019 (−0.249–0.172)	0.404 (−0.315–0.584)
4	TK	0.236 (−0.21–2.21)	−0.333 (−0.533–−0.101)	−0.345 (−0.701–0.154)	Cu	−0.066 (−0.459–0.339)	−0.279 (−0.426–0.299)	0.349 (−0.065–0.58)
3		0.377 (0.066–2.57)	−0.391 (−0.583–−0.074)	−0.217 (−0.616–0.057)		−0.081 (−0.479–0.24)	−0.054 (−0.369–0.379)	0.261 (−0.173–0.675)
2		0.116 (−0.376–0.626)	−0.217 (−0.491–0.066)	0.01 (−0.071–0.385)		−0.06 (−0.632–0.157)	−0.114 (−0.554–0.162)	−0.179 (−0.505–0.079)
1		−0.107 (−0.393–0.379)	0.101 (−0.302–0.846)	0.307 (0.076–0.343)		−0.364 (−0.73–−0.031)	−0.054 (−0.302–0.193)	0.06 (−0.41–0.334)
4	CaO	−0.971 (−0.995–−0.93)	−0.454 (−0.733–−0.192)	−0.36 (−0.607–1.35)	Zn	0.153 (−0.223–0.516)	−0.006 (−0.164–0.278)	0.125 (−0.042–0.851)
3		−0.987 (−0.994–−0.928)	−0.517 (−0.717–−0.141)	−0.563 (−0.68–1.02)		0.048 (−0.18–0.374)	−0.041 (−0.277–0.205)	−0.084 (−0.25–0.521)
2		−0.525 (−0.88–−0.165)	−0.286 (−0.418–0.131)	−0.193 (−0.382–−0.064)		−0.031 (−0.246–0.285)	0.195 (−0.11–0.451)	−0.133 (−0.394–0.227)
1		−0.646 (−0.969–−0.103)	−0.054 (−0.237–0.177)	0.225 (−0.414–0.866)		−0.093 (−0.573–0.018)	0.031 (−0.107–0.306)	−0.097 (−0.339–0.815)
4	MgO	−0.943 (−0.989–−0.824)	−0.349 (−0.457–−0.011)	−0.286 (−0.411–−0.158)	Mo	−0.347 (−0.813–−0.07)	1.146 (0.598–1.97)	0.572 (−0.114–0.807)
3		−0.954 (−0.991–−0.861)	−0.315 (−0.411–−0.06)	−0.242 (−0.381–−0.156)		−0.386 (−0.792–−0.221)	0.752 (0.035–1.14)	0.434 (−0.109–1.02)
2		−0.593 (−0.884–−0.04)	0.129 (−0.237–0.437)	0.05 (−0.213–0.381)		−0.38 (−0.734–0.019)	0.197 (−0.152–0.742)	−0.145 (−0.422–0.237)
1		−0.553 (−0.969–−0.018)	−0.03 (−0.114–0.254)	0.2 (−0.056–0.289)		−0.276 (−0.799–0.368)	0.128 (−0.135–0.339)	0.193 (0.025–0.302)

Table 4 continued

Profile	Elements	Mass transfer coefficient (τ)			Elements	Mass transfer coefficient (τ)		
		DGF	GGF	SGF		DGF	GGF	SGF
4	S	−0.441 (−0.835–−0.001)	0.677 (0.206–1.37)	0.78 (−0.104–5.21)	B	−0.092 (−0.627–0.575)	0.552 (−0.219–3.27)	−0.201 (−0.834–2.54)
3		−0.762 (−0.815–−0.418)	0.558 (−0.161–0.985)	0.795 (−0.406–2.54)		0.091 (−0.405–1.01)	−0.009 (−0.604–2.03)	−0.201 (−0.435–2.02)
2		−0.43 (−0.766–0.015)	−0.084 (−0.328–0.491)	−0.356 (−0.541–0.206)		0.044 (−0.3–0.213)	−0.39 (−0.67–0.3)	0.287 (−0.022–1.28)
1		−0.679 (−0.924–−0.016)	0.249 (−0.239–0.589)	−0.293 (−0.612–1.05)		0.045 (−0.829–0.327)	−0.042 (−0.505–0.858)	0.433 (−0.022–1.02)

1. Weak weathering layer; 2. Strong weathering layer; 3. Deep soil layer; 4. Topsoil layer

2008). Hence, weathering and pedogenesis process of the DGF in the study area can be summarized. In the early stage, the typical mobile elements in dolostone, Ca and Mg are significantly depleted during the whole weathering process. SiO_2 and Al_2O_3 comprised clay minerals and are retained in the soil. Fe and Mn initially occur in calcite, dolomite and accessory minerals as isomorphism. And then, with the dissolved of calcite, dolomite and accessory minerals, Fe is separated out and dominantly occurs as hydrate, oxide and hydroxide in soil, partly occurring as isomorphism in clay minerals. According to correlation analysis, highly significant positive correlations between Mn and SiO_2, Al_2O_3, Fe_2O_3, K_2O, and Ti are presented, with all the correlation coefficients more than 0.6 and the correlation coefficients to Fe being 0.726. During the weathering process, manganese compounds are partly oxidized to the hydroxides of Mn^{3+} or Mn^{4+}, and partly adsorbed by amorphous silica or clay minerals (Song et al. 2008; Tao et al. 2019). The former showed similar geochemical behaviors and evolution to Fe_2O_3. The mass transfer coefficient of Mn presents that it is mainly transferred outside the system during weathering, with the amount gradually dropping from the bottom. We guess that the amount of Mn released from Mn-rich dolomites may exceed the adsorption capacity of amorphous silicon and clay minerals, resulting in the loss of Mn at the early weathering stage. In addition, the pH values decrease gradually from bedrock to soil, with the average pH of the soil, regolith and bedrock being 7.71, 8.47, and 9.31, respectively, which contributed to the dissolution of Fe–Mn oxides or hydroxides. Mn accumulation in the topsoil by surface plants results in the gap between the geochemical behaviors of Mn and Fe. P has been released from accessory mineral, such as apatite, and then retained in weathering profile probably by being absorbed by Fe oxides or under the influence of biological behaviors (Liu et al. 2016). K and Na has been released from feldspar. The former may participate in forming clay minerals, such as illite at the early stage of weathering, and be retained in the soil as a composition of mica. In addition, K and Na have been retained in weathering profile probably by being absorbed by clay minerals or under the influence of biological behaviors (Jin et al. 2010).

Four factors of GGF interpreted 91.2% of the total variance of 10 variables studies (Table 5). Factor 1 (F1) is dominantly composed of SiO_2, Al_2O_3, Na_2O and K_2O, which SiO_2 and Al_2O_3 reflect the formation and evolution of clay minerals, while Na_2O and K_2O are subject to migration and depletion as mobile elements. Factor 2 (F2) is dominantly composed of FeO and MgO, both of that are occurred in clay as isomorphism and then migrate with the resolution of the clay minerals. Factor 3 (F3), dominantly composed of MnO and P_2O_5, suggest the impacts

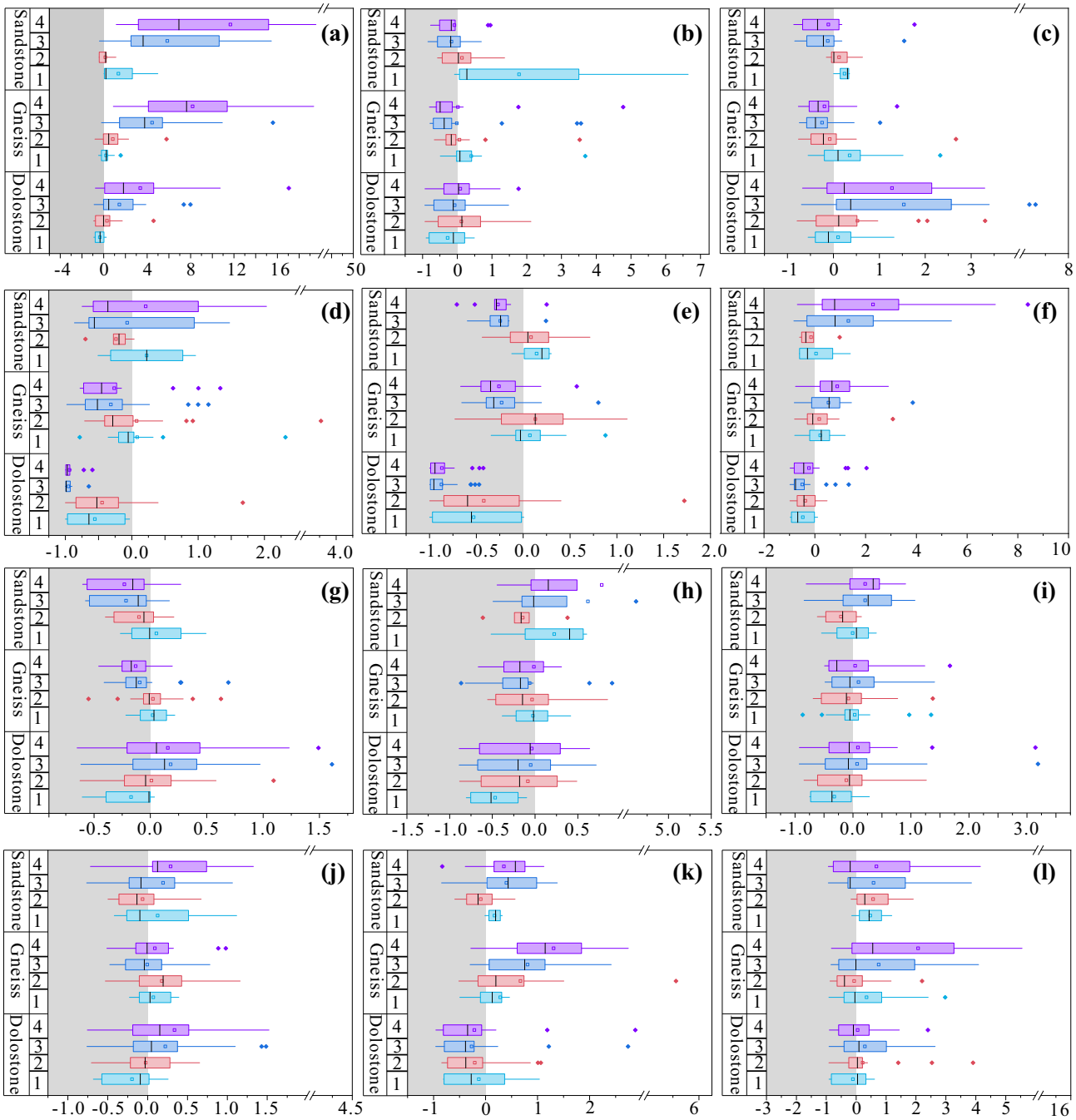

Fig. 5 Box plot of nutrient elements mass transfer of Earth's critical zone in Yanshan Mountain **a**.TN; **b**.TP; **c**.TK; **d**.CaO; **e**.MgO; **f**.S; **g**.Fe_2O_3; **h**.Mn; **i**.Cu; **j**.Zn; **k**.Mo; **l**. B 1. weak weathering layer; 2. strong weathering layer; 3. deep soil layer; 4. topsoil layer

performed by the supergene biogeochemical process. Factor 4 (F4), predominantly CaO, revealed the carbonate dissolutions. The weathering and pedogenesis process of crystalline rock is divided into four stages, from initial bedrock breaking to eventual ferralsol forming through migration of Soluble components, as well as the formation and evolution of clay minerals (Qiu et al. 2008). Weathering and pedogenesis of the GGF are analogously summarized as follows. First of all, acid solution flowed into bedrock through fractures, resulting in calcite dissolution and significant depletion of CaO. Secondly, alteration of plagioclase occurred as an important process in the weathering of gneiss (Biondino et al. 2020) so that Na_2O and CaO are separated from plagioclase and migrate through the solution, while SiO_2 and Al_2O_3 comprised clay minerals (Li et al. 2007). The dissolution of biotite,

Table 5 Factor analysis of major elements of Earth's critical zone in Yanshan Mountain

Factor	DGF			GGF				SGF			
	F1	F2	F3	F1	F2	F3	F4	F1	F2	F3	F4
SiO_2	0.821	0.437	0.191	0.921	0.091	0.28	0.112	−0.761	−0.21	−0.439	−0.319
TiO_2	0.767	0.38	0.45	–	–	–	–	0.82	0.426	0.038	0.1
Al_2O_3	0.892	0.168	0.333	0.917	0.155	0.28	0.085	0.652	0.211	0.346	0.589
Fe_2O_3	0.871	0.128	0.437	0.474	0.734	0.406	0.016	0.822	0.095	0.299	0.377
MgO	−0.743	−0.293	−0.486	−0.031	0.916	0.021	0.326	0.199	0.726	0.374	0.45
MnO	0.388	0.29	0.844	0.406	0.492	0.629	−0.022	0.571	0.18	0.777	−0.02
CaO	−0.914	−0.308	−0.04	0.162	0.234	0.069	0.945	0.134	0.914	0.329	0.032
Na_2O	0.401	0.873	0.104	0.861	0.156	0.342	0.219	0.302	0.88	−0.003	−0.193
K_2O	0.643	0.567	0.389	0.911	0.09	0.177	0.015	0.272	−0.072	0.022	0.936
P_2O_5	0.096	0.756	0.533	0.38	0.073	0.879	0.109	0.17	0.569	0.718	0.217
Accumulative variance contribution/%	75.6	85.7	91.8	42.5	61.8	80.1	92.1	59.9	78	86	92.4

hornblende contributed to the release of FeO, MgO, Na_2O, K_2O and CaO. Chloritization and damouritization occur along cleavage crack and margin of biotite and hornblende with the formation of iron oxide. Biotite and hornblende finally turned into clay minerals (Bazilevskaya et al. 2013), in which FeO and MgO occurred as isomorphism. It is followed by a minor amount of chlorite and potash feldspar. Eventually, when clay minerals are transferred or dissolved, FeO, MgO, Na_2O, and CaO are released and migrated as various inorganic cations or organic complexes (Shi et al. 2022). Accessory mineral weathering dominantly explains the Mn and P release at the early weathering stage (Liu et al. 2016). As the nutrient elements needed for vegetation growth, Mn and P have been influenced by surface biological processes.

Four varimax factors of SGF interpreted 92.4% of the total variance of 10 variables studies (Table 5). Factor 1 (F1) mainly comprised SiO_2, TiO_2, Al_2O_3, Fe_2O_3. SiO_2 is negatively correlated to factor 1, while others are positively correlated to factor 1. Aluminosilicates are almost decomposed so that mobile elements, including Si migrated and depleted, but Fe_2O_3 and Al_2O_3 occur as colloids under an acid environment (Qiu et al. 2008). Factor 2 (F2) mainly comprised CaO, Na_2O, and MgO, which are prone to migrate and deplete as soluble components. The former two elements have been released from plagioclase, while the latter may be related to the decomposition of sericite and other accessory minerals. Factor 3 (F3), mainly comprised of MnO and P_2O_5, revealed similar geochemical behavior and evolutions to GGF. Factor 4 (F4), mainly comprised of K_2O, suggests the decomposition of sericite or potassium feldspar.

4.3 Weathering influences the spatial structure of critical zone and distribution of vegetation community

4.3.1 The spatial structure of earth's critical zone

As mentioned above, bedrock weathering performed notable impacts on pedogenesis and eventually controlled the spatial structure of Earth's critical zone under identical climate conditions, such as bedrock fracture, the thickness of regolith and soil, and morphology of soil profile.

The steep hill is widely distributed in DGF with relative relief from 100 to 200 m. Dolostone is more resistant to physical weather because of its hardness and single mineral component while stronger chemical weathering than gneiss and sandstone. Soil is directly covered on tough bedrock without regolith in some typical weathering profiles driven by the shortage of soil-forming materials. In general, soil and regolith developed in DGF are relatively thin that the thickness of the soil is less than 10 cm and regolith is less than 30 cm. Secondary structural joints, dominated by the bedding and oblique joints, are developed in bedrock, which has super continuity or half-continuity. Low mountains and hills are formed in GGF with relative relief of less than 50 m. Gneiss is composed of various minerals which allowed strong physical weathering. Complete weathering profiles, including A, B, C and R layers, are developed in GGF, in which soil gradually transited to hard parent rock through loose regolith (Zhang and Li 1990). Both soil and regolith are thick. The thickness of the soil is more than 50 cm, and regolith ranges from 100 to 200 cm. Nontectonic joints, closely associated with weather, are developed

in bedrock, which is discontinuous. Low hills are developed in SGF with relative relief of less than 50 m. Quartz is abundant, and rock debris is dominated by silicalite in sandstone so that dolostone is weakly weathered in the region. Soil developed in SGF is a wide range of variations, in which the thickness of soil ranges from 30 to 50 cm, and regolith ranges from 50 to 100 cm. Nontectonic joints are slightly developed in superficial bedrock, which is discontinuous and like zigzag and step shape.

4.3.2 *Weathering influences the spatial structure of Earth's critical zone*

Weathering and pedogenesis of dolostone are composed of the accumulation of foreign and insoluble substances to saprolite and weathering of saprolite. Based on the in-suit weathering and pedogenesis of parent rock in the mountain areas, soil-forming materials are derived from weathering of bedrock. Carbonate minerals are transformed into bicarbonate and lost with the solution during dolostone weathering so that remanent materials are scarce (Zheng and Wang 2002; Guo and Li 2003). Thus, the soil formation rate of dolostone is slower while stronger weathering than gneiss and dolostone (Wang et al. 1999; Han and Liu 2004; Ma et al. 2010; West et al. 2013; Xu et al. 2013; Song et al. 2020). There is a general consensus that approximately 8000 years is needed to develop 1 cm soil in carbonate (Wang et al. 1999; Zhang et al. 2001). Therefore, thin soil and regolith are predominant in DGF. Gneiss is composed of various minerals whose expansion coefficients are significantly different, resulting in gneiss being subjected to physical weather. In addition, amphibole and biotite are liable to dissolve because of their small lattice energy. It is proposed that biotite content took a significant role in the thickness of soil as the expansion of biotite is one reason for thick regolith and soil development (Tian et al. 2019). On the other hand, joints are well developed in GGF, which contributes to more fissures or tiny fissures, offering space for vegetation roots. In return, water, O_2 and acid solution permeated downward into deep bedrock through fissures or vegetation roots, contributing to thick regolith and soil being developed with the thickness of several meters or even more than ten meters (Hu 1963; Anderson et al. 2007; Bazilevskaya et al. 2013; Biondino et al. 2020). Weathering rate of sandstone is slower than that of dolostone and gneiss because of the high content of quartz and weaker weather (Spatti júnior et al. 2019). In addition, weathering residues are almost sedimentations of detritus fragments from the parent rock, which is rich in sandy and gravel. Soil developed is characterized by abundant clay substance and poor permeability after hardening, which is subjected to being eroded (Zhang et al. 1991). Therefore, thin regolith and soil are predominantly developed in bedrock outcrops of SGF.

4.3.3 *Weathering influences the distribution of vegetation community*

As the lower boundary of Earth's critical zone, bedrock exerts potential impacts on the overlying vegetation by regulating the spatial structure of Earth's critical zone and soil property, and thus the suitability as a substrate for vegetation. On the one hand, bedrock offered most nutrients for vegetation, such as P, Ca, Mg, K and Fe, derived exclusively from minerals (Castle and Neff 2009). On the other hand, bedrock influenced water conservation in the regolith and soil and growth space for vegetation roots by controlling the thickness, porosity and fracture density of regolith and soil. Lithologic effects on vegetation are generally considered secondary to climatic factors such as the length of the growing season and the amount of moisture available for plant growth (Hahm et al. 2014; Jiang et al. 2020). Soil developed in DGF is thin but is typically rich in Ca. The vegetation community is dominated by rock plants that are calcivorous and more tolerant of barrenness (Hu 1963), such as *Biota Orientalis Endl*, *Vites incise Bunge, Spiraea trilobata Linn*. The vegetation community structure is relatively single and the positive successional rate of the ecological system is slow and apt to terminate (Yao et al. 2002; He et al. 2009). Soil developed in GGF is thick, intermediate-acid, and rich in nutrients, such as Fe, Mn, Zn, P, Cu, so that it is suitable for the arbors. There are widely high-quality economic forests, such as chestnut, hawthorn and walnut in GGF. According to previous studies, high-quality agricultural products are attributed to specific elements. For instance, high-quality chestnut, hawthorn, and walnut are respectively inclined to grow chiefly on Fe–Mn-rich acid soil, Fe–Mn-Zn-rich soils, and Ca-Zn-rich soils (Wen and Liu 2006; Wang et al. 2020). In addition, Fe and available potassium, followed by Zn and P, exert the heaviest influences on the fruit quality of apples according to the research on the apple planted in gneiss of Taihang mountain (Li et al. 2002). Hence, the wide spreading of high-quality chestnuts in GGF is also a natural selection. Soil developed in SGF, slightly acid with the average pH value of 5.92, shows heterogeneity in soil thickness that soil on the shady slopes is relatively thick while the soil in bedrock outcrops is thin. Macronutrients and micronutrients, such as N, P, K, Mn, Mo, as well as B, are enriched in the soil so that SGF is suitable for arbors on shady slopes with thick soil, while it is dominated by shrub on the sunny slope. It is observed that Chinese pines are widely spread in SGF, consistent with the summary of matching species with the site in Taihang Mountain that Chinese pine generally grows well in granitic gneiss,

sandstone and shale, especially on the shady slope since slightly acidic-neutral thick soil is beneficial for Chinese pine (Yang and Wang 1997).

5 Conclusions

1 Dolostone is the dominant rock type of DGF, composed of powdery dolomite, micritic dolomite and a low quantity of terrigenous sandy clastic materials. DGF is characterized by the strongest weathering and predominant chemical weathering in the region. Plagiogneiss is the dominant rock type of GGF whose mineral compositions are plagioclase, quartz, amphibole, biotite, and garnet. GGF is characterized by the weakest weathering and fast chemical and physical weathering rates. Sandstone is the primary rock type of SGF, composed of sandy fragments and interstitial material. The former is mainly quartz, feldspar and subangular rock debris, comprised of sericitization alteration rock, siliceous rock, as well as less quantity of mica. The latter is dominated by sericitization clay mixed base and siliceous rock. SGF is characterized by moderate weathering. In general, the region's weathering degree is relatively low, at the stage of kaolinization, early lateralization.

2 Soil is characterized by the illuviation of parent materials and the inherent origin of nutrients from parent rock. The migration and enrichment of elements during rock weathering and pedogenesis of three kinds of geological formations are significantly different. DGF is characterized by significant depletion of CaO, MgO, S, Mn, Mo and enrichment of N, K, Fe_2O_3, Zn with contents of P, Cu and B keeping stable. GGF is characterized by significant depletion of P, K, CaO, MgO, Fe_2O_3, Mn, Cu and enrichment of N, S, Mo and B, with contents of Zn keeping stable. SGF is characterized by significant depletion of P, K, CaO, MgO, Fe_2O_3, and enrichment of N, S, Mn, Cu, Zn, Mo, with fluctuant changes of Zn and B. R-mode factor analysis argues for liner correlational relationship between weathering and pedogenesis with element geochemical process.

3 Bedrock performed remarkable impacts on the spatial structure of Earth's critical zone and the distribution of vegetation community. Soil and regolith developed in DGF are thin that the thickness of the soil is less than 10 cm and regolith is less than 30 cm. The vegetation community is predominantly rock plants that are calcivorous and tolerant of barren, such as *Biota Orientalis Endl*, *Vites incise Bunge, Spiraea trilobata Linn*. Both soil and regolith developed in GGF are thick. The thickness of the soil is more than 50 cm, and regolith ranges from 100 to 200 cm, suggesting its suitability for arbors. The vegetation community is predominantly high-quality economic forests, such as chestnut, hawthorn and walnut, as well as various arbors because of the enrichment of nutrients in GGF. The thickness of soil developed in SGF varies between that of DGF and GGF which the thickness of soil ranges from 30 to 50 cm and regolith ranges from 50 to 100 cm. Chinese pines are widespread in thick soil developed on the shady slope of SGF.

Acknowledgements This research was funded by the Research Program of Tianjin North China Geological Exploration Bureau (No. HK2021-B15), and additional supporting was provided by the Geological Survey Program of China Geological Survey, Ministry of Natural Resources (No. DD20190822) and S&T Program of Hebei (CN) (No. 19224205D).

Funding Research Program of Tianjin North China Geological Exploration Bureau, HK2021-B15, Daqing Fu, Geological Survey Program of China Geological Survey,Ministry of Natural Resources, DD20190822, Xiaofeng Wei, S&T Program of Hebei (CN), 19224205D, Hao Wei.

Declarations

Conflict of interest The authors declare that they have no conflict of interest.

References

Anderson SP, Dietrich WE, Brimhall GH (2002) Weathering profiles, mass-balance analysis, and rates of solute loss: Linkages between weathering and erosion in a small, steep catchment. Geol Soc Am Bull 114 (9):1143–1158. https://doi.org/10.1130/0016-7606

Anderson SP, von Blanckenburg F, White AF (2007) Physical and chemical controls on the critical zone. Elements 3 (5):315–319. https://doi.org/10.2113/gselements.3.5.315

Bazilevskaya E, Lebedeva M, Pavich M, Rother G, Parkinson DY, Cole D, Brantley S (2013) Where fast weathering creates thin regolith and slow weathering creates thick regolith. Earth Surf Process Landf 38 (8):847–858. https://doi.org/10.1002/esp.3369

Biondino D, Borrelli L, Critelli S, Muto F, Apollaro C, Coniglio S, Tripodi V, Perri F (2020) A multidisciplinary approach to investigate weathering processes affecting gneissic rocks. Catena 187:1–17. https://doi.org/10.1016/j.catena.2019.104372

Brantley SL, Goldhaber MB, Ragnarsdottir KV (2007) Crossing disciplines and scales to understand the critical zone. Elements 3 (5):307–314. https://doi.org/10.2113/gselements.3.5.307

Castle SC, Neff JC (2009) Plant response to nutrient availability across variable bedrock geologies. Ecosystems 12 (1):101–113. https://doi.org/10.1007/s10021-008-9210-8

Chadwick OA, Brimhall GH, Hendricks DM (1990) From a black to a gray box — a mass balance interpretation of pedogenesis. Geomorphology 3 (3):369–390. https://doi.org/10.1016/0169-555X(90)90012-F

Chen LP (2019) Study of weathering intensity in the critical zone and its influence factors across heihe drainage basin. Dissertation, Lanzhou university

Cheng HX, Peng M, Zhao CD, Han W, Wang HY, Wang QL, Yang F, Zhang FG, Wang CW, Liu F, Zhou YL, Tang Q, Li K, Yang K, Yang Z, Cheng XM, Chen ZW, Zhang H, Mo CH (2019) Epigenetic geochemical dynamics and driving mechanisms of distribution patterns of chemical elements in soil southwest china. Earth Sci Front 26 (6):159–191

Clift PD, Wan S, Blusztajn J (2014) Reconstructing chemical weathering, physical erosion and monsoon intensity since 25 Ma in the northern South China Sea A review of competing proxies. Earth Sci Rev 130:86–102. https://doi.org/10.1016/j.earscirev.2014.01.002

Dixon JL, Chadwick OA, Vitousek PM (2016) Climate-driven thresholds for chemical weathering in postglacial soils of new zealand. J Geophys Res: Earth Surf 121 (9):1619–1634. https://doi.org/10.1002/2016JF003864

Fang Q, Hong HL, Zhao LL, Cheng F, Yin K, Wang CW (2018) Climatic implication of authigenic minerals formed during pedogenic weathering processes. Earth Sci 43 (3):753–769

Fu HJ, Jian X, Liang HH (2021) Research progress of sediment indicators and methods for evaluation of silicate chemical weathering intensity. J Palaeogeogr (Chinese Edition) 23 (6):1192–1209

Goldich SS (1938) A study in rock-weathering. J Geol 46 (1):17–58. https://doi.org/10.1086/624619

Gu T, Zheng XZ, Qiu XF, Jiang T, Zhao XW, Shuai Q (2021) Element geochemical characteristics of mesozoic granite weathering crust profile in Shenwan Town Zhongshan City, South China Geol 37 (4):406–417

Guan XY, Guo J, Chen HY, Xiu D, Zhang YQ (2018) Discovery of stromatolites from the Ordovician Yeli Formation and its sedimentary environment in Chengde basin, Hebei province. Adv Earth Sci 33 (5):545–553

Guo JJ, Li HZ (2003) Analysis and research on the soil characteristics of different parent rocks and materials. J Hebei For Sci Technol 2:7–8

Hahm WJ, Riebe CS, Lukens CE, Araki S (2014) Bedrock composition regulates mountain ecosystems and landscape evolution. Proc Natl Acad Sci U S A 111 (9):3338–3343. https://doi.org/10.1073/pnas.1315667111

Hahm WJ, Rempe DM, Dralle DN, Dawson TE, Lovill SM, Bryk AB, Bish DL, Schieber J, Dietrich WE (2019) Lithologically controlled subsurface critical zone thickness and water storage capacity determine regional plant community composition. Water Resour Res 55 (4):3028–3055. https://doi.org/10.1029/2018WR023760

Han GL, Liu CQ (2004) Water geochemistry controlled by carbonate dissolution: a study of the river waters draining karst-dominated terrain, Guizhou Province China. Chem Geol 204 (1):1–21. https://doi.org/10.1016/j.chemgeo.2003.09.009

Hao LB, Ma L, Zhao HB (2004) Elemental homogenization during weathering and pedogenesis of volcanic rocks from North Dahingganling. Geochimica 33 (2):131–138

Hao LB, Lu JL, Ma L (2005) Relation between the chemical compositions of residual soils and bedrocks in shallow overburden areas and its significance-a case study of the northern Dahinggan mountains. Chin Geol 32 (3):477–482

He YB, Zhang XB, Wen AB (2009) Discussion on karst soil erosion mechanism in karst mountain area in southwest China. Ecol Environ Sci 18 (6):2393–2398

He ZX, Fan LY, Wei XF, Gan FW, Li DJ, Chai X (2020) Large-scale survey of geological heritage in the panlong lake area of Chengde, Hebei province: based on geological formations and watershed landforms. Geol China 47 (6):1881–1893

Hewaisam T, von Blanckenburg F, Bouchez J, Dixon JL, Schuessler JA, Maekeler R (2013) Slow advance of the weathering front during deep, supply-limited saprolite formation in the tropical highlands of Sri Lanka. Geochim et Cosmochim Acta 118 (1):202–230. https://doi.org/10.1016/j.gca.2013.05.006

Hodson ME, Langan SJ, Wilson MJ (1996) A sensitivity analysis of the profile model in relation to the calculation of soil weathering rates. Appl Geochem 11 (6):835–844. https://doi.org/10.1016/S0883-2927(96)00048-0

Hong HL, Du DW, Li RB, Churchman JG, Yin K, Wang CW (2012) Mixed-layer clay minerals in the Xuancheng red clay sediments, Xuancheng Anhui Province. Earth Sci (Journal of China University of Geosciences) 37 (3):424–432

Hu TK (1963) The soil conservation of the middle region of Da-lin river, west part of Liaoning province with different types of relief and parent materials. J Shenyang Agric Univ 4:124–130

Huang ZG, Zhang WQ, Liu RH (1996) Red weathering crust in southern China. Ocean Press, Beijing

Jiang Z, Liu H, Wang H, Peng J, Meersmans J, Green SM, Quine TA, Wu X, Song Z (2020) Bedrock geochemistry influences vegetation growth by regulating the regolith water holding capacity. Nat Commun 11 (1):1–9. https://doi.org/10.1038/s41467-020-16156-1

Jin JH, Li ZZ, Chen XL, Ling ZY, Cao XD, Wang SP (2010) Major elements in aeolian sediments of the late holocene in yili valley and their climatic implications. J Palaeogeogr 12 (6):675–684

Li BG, Qi GH, Guo SP, Li HZ, Zhang LP (2002) Study on the relationship between the soil nutrient elements and the apple fruit quality of the newly reclaimed apple orchard in Taihang mountain gneiss area. Chin J Eco Agric 10 (3):21–24

Li XS, Han ZY, Yang SY, Chen YY, Wang YB, Yang DY (2007) Chemical weathering intensity and element migration features of the Xiashu Loess profile in zhenjiang. Acta Geogr Sin 62 (11):1174–1184

Li J, Liang HB, Wan X, Dong JX, Li DC, Xu YM, Wu YH, Chen XD, Peng D, Xu M, Wang ZX (2013) Relationship between tobacco soil nutrients and soil parent materials. Chin Tob Sci 34 (3):21–25

Liao SG (1997) The relation between the characteristics of rocks and soil erosion in Hetian. J Fujian Teach Univ (Natural Science) 13 (2):102–108

Liu WJ, Liu CQ, Brantley SL, Xu ZF, Zhao T, Liu TZ, Yu C, Xue DS, Zhao ZQ, Cui LF, Zhang ZJ, Fan BL, Gu X (2016) Deep weathering along a granite ridgeline in a subtropical climate. Chem Geol. https://doi.org/10.1016/j.chemgeo.2016.02.014

Lo FL, Chen HF, Fang JN (2017) Discussion of suitable chemical weathering proxies in sediments by comparing the dissolution rates of minerals in different rocks. J Geol 125 (1):83–89. https://doi.org/10.1086/689184

Łukasz P, Phillips JD, Pavel Š (2016) Roots, rock, and regolith: biomechanical and biochemical weathering by trees and its impact on hillslopes—a critical literature review. Earth-Sci Rev 159 (1):142–159. https://doi.org/10.1016/j.earscirev.2016.06.002

Lv YZ, Li BG (2006) Edaphology. China Agriculture Press, Beijing

Ma L, Hao LB, Pan J, Liu HT, Duan GZ (2003) Geochemistry of rhyolite weathering of alongshan, Greater Xing'an mountains. J Jilin Univ 33 (3):296-299 314

Ma L, Chabaux F, Pelt E, Blaes E, Jin L, Brantley S (2010) Regolith production rates calculated with uranium-series isotopes at susquehanna/shale hills critical zone observatory. Earth Planet Sci Lett 297 (1):211–225. https://doi.org/10.1016/j.epsl.2010.06.022

Meybeck M (1987) Global chemical weathering of surficial rocks estimated from river dissolved loads. Am J Sci 287 (5):401–428. https://doi.org/10.2475/ajs.287.5.401

Nesbitt H, Young G (1984) Prediction of some weathering trends of plutonic and volcanic rocks based on thermodynamic and kinetic considerations. Geochim et Cosmochim Acta 48 (7):1523–1534. https://doi.org/10.1016/0016-7037(84)90408-3

Nie HF, Xiao CL, Dai M, Liu JY, Shang BX, Guo ZC, He P, Ouyang Y, Lei TC, Li WM, Zhou CF, Jiang QG (2021) Progresses and main achievements of ecogeological survey project. Geol Surv China 8 (1):1–12

Qiu T, Qiu YX, Zheng CQ, Hu F (2008) The silicate solution and the soil formation process. Guizhou Geol 25 (1):51–58

Shi JS, Ma R, Ma Z (2019) Regional investigation of the Earth's critical zone. Acta Geosci Sin 40 (6):767–780

Shi WW, Yang ZL, Yin HG, Niu JH, Du GC, Chen J, Chen YY, Cui YK (2022) Characteristics and formation mechanism of sandstone spherical weathering in lower cambrian qiongzhusi formation micangshan structural zone. Glob Geol 41 (1):173–185

Song ZL, Zhu ZZ, Yang C, Wu YF (2008) Mobility and enrichment of manganese and phosphorus during limestone weathering in the wujiang catchments of southwestern china. J Zhejiang For Coll 25 (6):705–710

Song ZL, Zhang H, Luo WJ, Liu TZ (2020) Soil evolution and its controlling mechanisms in a critical zone. Bull Mineral Petrol Geochem 39 (1):24–29

Spatti Júnior EP, da Conceição FT, Fernandes AM, Sardinha DDS, Menegário AA, Moruzzi RB (2019) Chemical weathering rates of clastic sedimentary rocks from the paraná basin in the paulista peripheral depression, brazil. J South Am Earth Sci 96:1–12. https://doi.org/10.1016/j.jsames.2019.102369

Sun ZM (2018) Silicate weathering rate and its controlling factors: the study from the different "small watershed systerms". Dissertation, nanjing university

Sun HY, Wei XF, Sun XM, Jia FC, Li DJ, Li J (2020) Element migration and accumulation characteristics of bedrock-regolith-soil-fruit plant continuum of the Earth's critical zone in chengde almond producing area. Earth Sci 46 (7):2621–2645

Tao JM, Wang JG, Liu XY, Han YJ, Liu ZC (2019) Migration characteristics of mineral elements between Suizhong granites and brunisolic soils in Xingcheng area, Liaoning province. China Glob Geol 38 (3):636–642

Tian Z, Hartsough PC, O'Geen AT (2019) Lithologic, climatic and depth controls on critical zone transformations. Soil Sci Soc Am J 83 (2):437–447. https://doi.org/10.2136/sssaj2018.03.0120

Wang SJ, Ji HB, Ouyang ZY, Zhou DQ, Zheng LP, Li TY (1999) Preliminary research on the weathering and pedogenesis of carbonatite. Sci China (Series D) 29 (5):441–449

Wang ZG, Wan MC, Sun JJ, Zhang PC (2015) Review of studies on soil formation rate in karst rocky desertification region of southwest china. J Yangtze River Sci Res Inst 32 (3):64–72

Wang JB, Wei XF, Zhang HQ, Gan FW (2020) The eco-geological survey based on geological formation, exemplified by integrated geological survey of national ecological civilization demonstration area in Chengde City Hebei Province. Geol China 47 (6):1611–1624

Wei XF, Fan LY, Sun ZJ, He ZX, Sun HY, Wei H (2020) The influence of geological formation on plant community composition in Chaibai River Basin, Chengde, Hebei Province. Geol China 47 (6):1869–1880

Wen D, Liu SQ (2006) The impaction of climate and site condition on the growth and fruiting of Chinese chestnut. Hebei J For Orchard Res 21 (4):434–437

West N, Kirby E, Bierman P, Slingerland R, Ma L, Rood D, Brantley S (2013) Regolith production and transport at the susquehanna shale hills critical zone observatory, part 2: insights from meteoric ^{10}Be (Article). Geophys Res Earth Surf 118 (3):1877–1896. https://doi.org/10.1002/jgrf.20121

Xiao CL, Nie HF, Liu JY, Yuan GL, Kang YH, Wang AT, Song BF (2021) Ecological and geological interaction model: The coupling of supergene geological processes and ecological characteristics. Geol Sur China 8 (6):9–24

Xu HJ, Ma CQ (2002) Review on weathering rates in the crust weathering system. Adv Earth Sci 17 (5):670–678

Xu S, Liu CQ, Freeman S, Lang YC, Schnabel C, Tu CL, Wilcken K, Zhao ZQ (2013) In-situ cosmogenic ^{36}Cl denudation rates of carbonates in Guizhou karst area. Chin Sci Bull 58 (20):2473–2479. https://doi.org/10.1007/s11434-013-5756-8

Yang JG, Wang HX (1997) Research on matching species with the site in Taihang mountain. For Resour Manag 1:19–26

Yang JX, Liu CQ, Zhao ZQ, Ding H, Liu TZ, Tu CL, Fan BL, Huang L (2016) Geochemical behavior of rare-earth element during the weathering of granite under different climatic conditions. Acta Mineral Sin 36 (1):125–137

Yao Z, Zhang P, Liu AM (2002) Relationship between the karst regional geomorphy and the virgin forest: a case study of maolan at Libo and Mashan at Wangmo, Guizhou. Guizhou Geol 19 (2):99–102

Yin ZQ, Wei XF, Liu WB, Li X, Xing YM, Chen L, Wang RF, Yang R, Ma GW, Peng C (2020) Progresses and main achievements of comprehensive geological survey project of natural resources in Chengde. Geol Surv China 7 (3):1–12

Yuan GX, Shang YJ, Yang ZF (2010) Analysis of rock weathering rate and influencing factors in Bomi region, southeast Tibet. J Eng Geol 18 (2):191–196

Zhang FR, Li LJ (1990) Genetic characteristics and properties of soils developed from two kind of rocks in the low-mountain area of Beijing. Acta Agric Univ Pekin 16 (2):161–167

Zhang JG, Li YR, Zhao HJ (1991) The basic laws of soil erosion in the haihe river watershed of Shanxi province. Bull Soil Water Conserv 5:17–25

Zhang DF, Wang SJ, Zhou DQ, Li RL (2001) Intrinsic driving mechanism of land rocky desertification in karst regions of Guizhou province. Bull Soil Water Conserv 21 (4):1–5

Zhang ML, Yang H, Zou J, Xu LJ, Sui ZL (2011) Effects of soil erosion on soil quality in the rocky mountain areas of northern China. J Soil Water Conserv 25 (2):218–221

Zhang YQ, Chen HY, Wei WT, Chen C, Liu YL, Zhang LG, Zhu ZP (2014) The tuffs from the jiulongshan formation in the Chengde Basin, northern Hebei: LA-ICP-MS zircon U-Pb age dating and its geological implications. Sediment Geol Tethyan Geol 34 (3):88–95

Zhang TJ, Liu H, Ouyang Y, Zhang JH, Zhang ZJ, Li T (2021) Ecological environment function of different geological formations: a case study of Xichang area. Geol Surv China 8 (6):35–49

Zhao SY, Li M, Suo GB (2022) Research on sustainable development of resource-based city from an arbitrary viewing point. China Mark 2:23-24 37

Zhao LP (2007) Study on theories of forest vegetation recovery and construction in Yanshan mountain area. Dissertation, Nanjing Forestry University

Zheng YC, Wang SJ (2002) Geological cause of calcareous soil erosion and land rocky desertification in karst area, Guizhou Province. Resour Environ Yangtza Basin 11 (5):461–465

Zhou DQ, Wang SJ, Liu XM (2005) Study on geochemical processes in limestone soil profiles. Geol Geochem 33 (2):31–38

Zhu LJ, Li JY (2006) Weathering and pedogenesis of carbonate and its environmental effects. Geology Press, Beijing